JACS
JOURNAL OF THE AMERICAN CHEMICAL SOCIETY
Article
pubs.acs.org/JACS

From Blue to Green: Fine-Tuning of Photoluminescence and Electrochemiluminescence in Bifunctional Organic Dyes

Fabio Rizzo,*[,†,‡] Federico Polo,*[,§,#] Gregorio Bottaro,[∥] Simona Fantacci,[⊥] Sabrina Antonello,[§] Lidia Armelao,[§,∥] Silvio Quici,[‡] and Flavio Maran*[,§]

[†]Institute of Molecular Science and Technologies (ISTM), National Research Council (CNR), PST-CNR, via Fantoli 16/15, 20138 Milano, Italy

[‡]Institute of Molecular Science and Technologies (ISTM), National Research Council (CNR), and INSTM, c/o Department of Chemistry, University of Milano, via Golgi 19, 20133 Milano, Italy

[§]Department of Chemistry, University of Padova, via Marzolo 1, 35131 Padova, Italy

[∥]Institute of Condensed Matter Chemistry and Technologies for Energy (ICMATE), National Research Council (CNR), c/o Department of Chemistry, University of Padova, via Marzolo 1, 35131 Padova, Italy

[⊥]Institute of Molecular Science and Technologies (ISTM), National Research Council (CNR), c/o Department of Chemistry, University of Perugia, via Elce di Sotto 8, 06123 Perugia, Italy

Supporting Information

ABSTRACT: We describe the synthesis, computational analysis, photophysics, electrochemistry and electrochemiluminescence (ECL) of a series of compounds formed of two triphenylamines linked by a fluorene or spirobifluorene bridge. The phenylamine moieties were modified at the *para*-position of the two external rings by electron-withdrawing or electron-donating substituents. These modifications allowed for fine-tuning of the photoluminescence (PL) and ECL emission from blue to green, with an overall wavelength span of 73 (PL) and 67 (ECL) nm, respectively. For all compounds, we observed a very high PL quantum yield (79−89%) and formation of stable radical ions. The ECL properties were investigated by direct annihilation of the electrogenerated radical anion and radical cation. The radical-ion annihilation process is very efficient and causes an intense greenish-blue ECL emission, easily observable even by naked eye, with quantum yield higher than the standard 9,10-diphenylanthracene. The ECL spectra show one single band that almost matches the PL band. Because the energy of the annihilation reaction is higher than that required to form the singlet excited state, the S-route is considered the favored pathway followed by the ECL process in these molecules. All these features point to this type of molecular system as promising for ECL applications.

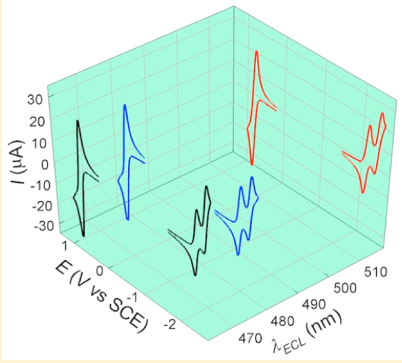

INTRODUCTION

In electrochemically generated chemiluminescence or electrochemiluminescence (ECL), electrochemical activation of suitable molecules or ions generates species that undergo sufficiently exergonic electron-transfer (ET) reactions to form excited state species (emitters) capable of causing luminescence.[1] The ECL reaction mechanism may involve formation of an excited singlet state via a direct annihilation of the radical ions generated from a species A by stepping the electrode potential at appropriate positive and negative values (eqs 1−4). The two ECL-active radical ions may be electrogenerated also by using two different molecules.

$$A - e \rightarrow A^{\bullet +} \quad (1)$$

$$A + e \rightarrow A^{\bullet -} \quad (2)$$

$$A^{\bullet +} + A^{\bullet -} \rightarrow {}^1A^* + A \quad (3)$$

$${}^1A^* \rightarrow A + h\nu \quad (4)$$

Reaction 3 is favored over an ET reaction that directly forms the neutral species in their ground-state; this is because the latter falls in the Marcus inverted region in which the ET rate decreases as the reaction becomes very exergonic.[2] The mechanism shown in eqs 1−4 is defined as the "S-route" because a singlet state $^1A^*$ is directly generated. Systems with insufficient energy follow the "T-route", in which a triplet state is produced first (eq 5) and then a triplet−triplet annihilation step generates the singlet excited state $^1A^*$ (eq 6) that emits light (eq 4).

$$A^{\bullet +} + A^{\bullet -} \rightarrow {}^3A^* + A \quad (5)$$

$${}^3A^* + {}^3A^* \rightarrow {}^1A^* + A \quad (6)$$

Received: November 28, 2016
Published: January 15, 2017

DOI: 10.1021/jacs.6b12247
J. Am. Chem. Soc. 2017, 139, 2060−2069

Alternatively to the S-route and the T-route, ion-annihilation reactions may lead to formation of excimers (eq 7) or exciplexes (eq 8):

$$A^{\bullet+} + A^{\bullet-} \rightarrow A_2^* \quad (7)$$

$$A^{\bullet+} + B^{\bullet-} \rightarrow (AB)^* \quad (8)$$

where B represents a second electroactive molecule. A further ECL pathway relies on the use of a coreactant liable to produce a strong reducing or oxidizing species.[3] For example, dibenzoyl peroxide undergoes concerted reductive cleavage of the O−O bond[4,5] to form a carboxylate RO^- but also the strong oxidant $RO^{\bullet}$.[4]

Since its early development, ECL found particular use as an analytical tool because the light intensity is proportional to the concentration of the emitting species.[6,7] For example, ECL provides a convenient detection approach in immunoassays.[8] Other applications regard light-emitting devices based on liquid emitting materials, such as liquid organic light-emitting diodes (liquid-OLED),[9,10] ECL cells,[11] and light-emitting electrochemical cells (LECs),[12] which can provide self-emission under appropriate voltage conditions. Ruthenium polypyridyl complexes, especially ruthenium(II) tris(bipyridine), are the most widely used ECL emitters, especially in biorelated applications. However, there is an increasing demand for the synthesis, characterization and application of new ECL materials, such as organic dyes,[13−15] metal complexes (mainly iridium[16−18] and platinum[19]), and nanoparticles,[20−22] that could emit at wavelengths other than those typical of ruthenium complexes. Devising systems that could allow for fine-tuning of the emission wavelength holds a tremendous potential for future applications of multicolor ECL.[18−20,23,24] In this context, it has been shown that the emission color can be modified using a combination of ruthenium(II) and iridium(III) complexes.[24] Arguably, however, organic compounds could offer a more general answer to this challenge particularly because of their chemical versatility and, therefore, the possibility of modulating electronic and photophysical properties precisely. Organic molecules have been designed and synthesized for ECL purposes,[25−28] but few systematic studies focused on substituent effects on the ECL emission energy and efficiency.[29−32] Recently, we described the photophysical and ECL properties of compounds obtained by linking two triphenylamine moieties to fluorene or spirobifluorene.[33] These compounds showed intense blue photoluminescence (PL) and ECL emission with high quantum efficiency.

Here we describe the synthesis, photophysics, electrochemistry, and computational study of two series of compounds containing triphenylamines and fluorene or spirobifluorene moieties. The triphenylamine groups were substituted at the *para* positions of the external rings with electron-withdrawing or electron-donating groups (Chart 1). ECL was triggered by direct annihilation of the radical ions electrogenerated by pulsing the electrode potential between positive and negative values. This study shows that effective fine-tuning of the PL and ECL behavior is made possible by chemically assembling luminophore systems that display bifunctional redox features, i.e., systems in which the electroreducible and electrooxidizable moieties are, to a large extent, decoupled.

EXPERIMENTAL SECTION

Full experimental details for the preparation and characterization of compounds **1**−**6** are provided in the Supporting Information.

Chart 1. Structures of the Investigated Compounds

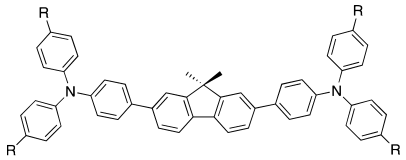

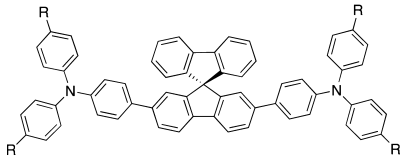

Spectroscopic Characterization. The UV−vis absorption spectroscopy measurements were carried out in anhydrous, freshly distilled DMF solutions by using a double-beam CARY5E spectrophotometer with a spectral bandwidth of 1 nm. The emission spectra were obtained with a Fluorolog-3 (Horiba Jobin Yvon) spectrofluorimeter equipped with double-grating monochromator in both the excitation and emission sides, and coupled to a R928P Hamamatsu photomultiplier; a 450 W Xe arc lamp was used as the excitation source. The emission spectra were corrected for detection and optical spectral response of the spectrofluorimeter through a calibration curve supplied by the manufacturer. Absolute photoluminescence quantum yields (QY_{PL}) were calculated by corrected emission spectra obtained with an apparatus consisting of a Spectralon coated integrating sphere accessory (4″, F-3018, Horiba Jobin Yvon), fitted in the fluorimeter sample chamber. For each compound, three independent measurements were carried out, with an estimated error of ±20%. Quantum-yield values were independent of the excitation wavelength in the investigated range. Photoluminescence lifetimes in the ns range were measured with a time-correlated single-photon counting device (Fluorohub-b, Horiba Jobin-Yvon) coupled with Fluorolog-3, using pulsed NanoLED excitation sources at 295 nm (pulse width ≤1 ns). Analysis of the luminescence decay profiles vs time was accomplished with the DAS6 Decay Analysis Software provided by the manufacturer. Experimental uncertainties in the lifetime determinations are estimated to be 10%.

Electrochemistry. DMF (Sigma-Aldrich, 99.8%) was treated with anhydrous Na_2CO_3 and then doubly distilled at reduced pressure under a nitrogen atmosphere. Tetra-*n*-butylammonium perchlorate (TBAP, Fluka, 99%) was recrystallized from a 2:1 ethanol−water solution and dried at 60 °C under vacuum. The working electrode was a homemade glassy-carbon disk electrode (3 mm diameter, Tokai GC-20) connected to a copper wire with silver epoxy and sealed in a PEEK body. The electrode was polished as already described.[34] Before experiments, the electrode was further polished with a 0.25 μm diamond paste (Struer) and electrochemically activated in the background solution by means of several voltammetric cycles at 0.5 V s^{-1} between the anodic and the cathodic solvent/electrolyte discharges, until the expected quality features were attained.[35] A platinum wire served as the counter electrode and a silver wire, separated from the main electrolytic compartment by a Vycor frit, was used as a quasi-reference electrode. At the end of each experiment, its potential was calibrated against the ferricenium/ferrocene couple, used as an internal redox standard. In DMF/0.1 M TBAP, ferricenium/ferrocene has a formal potential of 0.464 V against the KCl saturated calomel electrode (SCE);[34] all potentials will be given against SCE. The cyclic voltammetry (CV) experiments were carried out in DMF/0.1 M TBAP, using a 1 mM concentration for the electroactive compound. The diffusion coefficient values were determined with reference to that of ferrocene, which in this solvent/electrolyte system is 1.13×10^{-5} cm^2 s^{-1}.[35] The CV and ECL experiments were conducted at 25 °C under an Ar atmosphere using a cell consisting of

DOI: 10.1021/jacs.6b12247
J. Am. Chem. Soc. 2017, 139, 2060−2069

Scheme 1. Synthetic Route for the Synthesis of 1 and 2

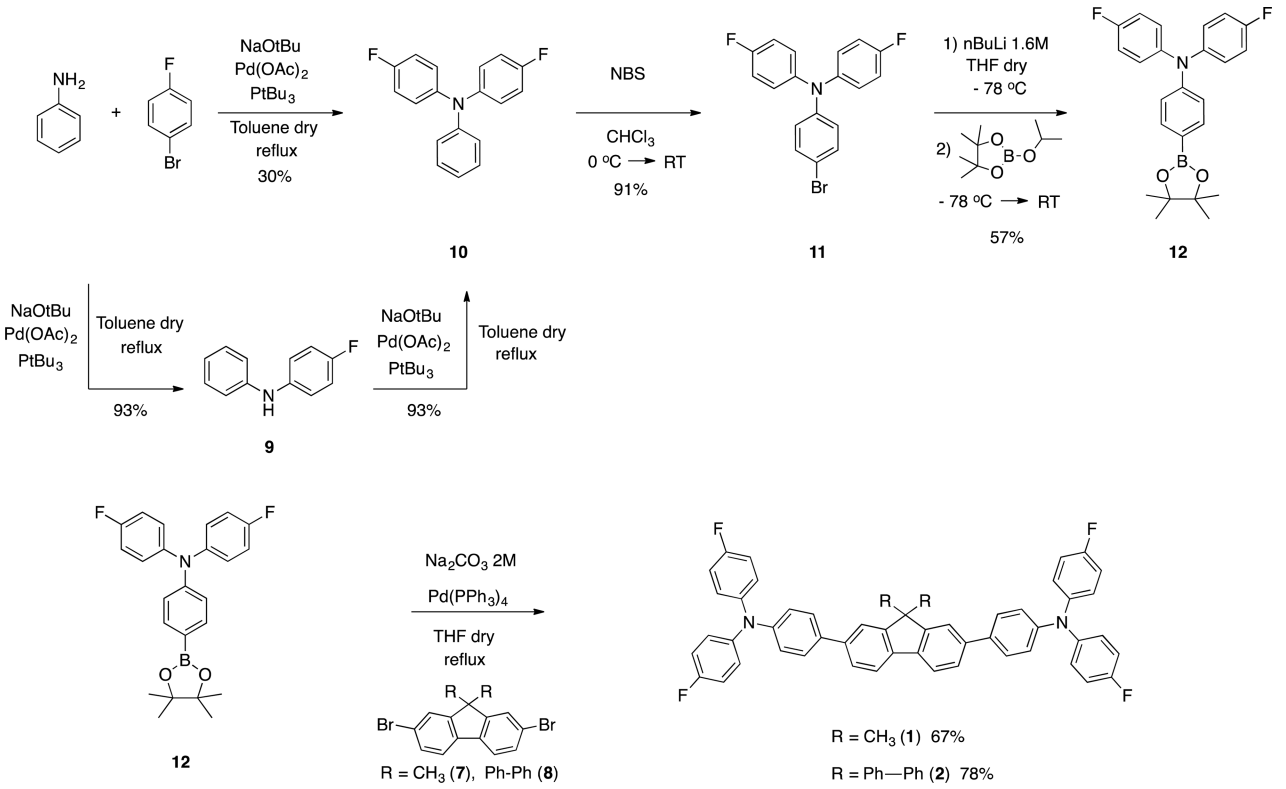

a purposely modified quartz cuvette. A CHI 760D Electrochemical Workstation (CH Instruments) was used. For the CV experiments, we employed the feedback correction to minimize the ohmic drop between the working and the reference electrodes.

Computational Details. Density functional theory (DFT) methods, including time-dependent DFT (TDDFT), were used to model the spirobifluorene systems' properties. Calculations were performed by using the software Gaussian09 (G09).[36] The molecular structure of **2**, **4**, **6** and **18** (in which the triphenylamines are unsubstituted on the external rings) were optimized without any symmetry constraints by using M06 as exchange correlation functional[37] and 6-31g** as basis set.[38] For all species, we optimized the ground state (S_0) geometry and the lowest singlet (S_1) excited state geometry. The geometry optimizations were performed in vacuo and with a polarizable continuum model of the solvent (DMF, $\varepsilon = 37$), as implemented in G09.[39]

ECL. The ECL experiments were conducted using the same electrochemical cell configuration as described above. The glassy-carbon electrode was polished and activated and then positioned a few millimeters from the photomultiplier tube (PMT). The reference and the counter electrodes were the same. ECL transients were recorded using a CHI 1040B electrochemical workstation (CH Instruments) coupled with a photosensor module equipped with a PMT (Hamamatsu, H10723−20). The pulsing potential was set to 100 mV past the peak potentials of the oxidation wave and the first or second reduction wave. The pulse width was 25 ms, unless otherwise stated. The photocurrent detected by the PMT was converted to a voltage signal through the photosensor module and acquired by the external input channel of the analog-to-digital converter (ADC) of the CHI 1040B workstation. The transients and the faradic currents were managed by using the software provided with the CHI workstation. The ECL spectra were acquired using a calibrated electron multiplying charge couple device (EM-CCD) camera (Andor technology, Newton EM-CCD) coupled with a spectrograph (Andor Technology, Shamrock 163). ECL emission was also recorded with an 8 MP camera of iPhone 4s (Apple).

RESULTS AND DISCUSSION

Synthesis. The syntheses were carried out according to strategies that share the step consisting in the preparation of the core (9,9-dimethyl-9*H*-fluorene and 9,9′-spirobifluorene) bearing two bromine atoms in position 2 and 7 (compounds **7**[40] and **8**[41]).

The synthesis of 2,7-bis(4-(*N*,*N*-bis(4-fluorophenyl)amino)-phen-1-yl)-9,9-dimethyl-9*H*-fluorene (**1**) and 2,7-bis(4-(*N*,*N*-bis(4-fluorophenyl)amino)phen-1-yl)-9,9′-spirobifluorene (**2**) (Scheme 1) was achieved through Suzuki coupling between the core (compounds **7** or **8**) and the boronic ester of the fluorinated triphenylamine (**12**). Introduction of fluorine on the *para*-position of triphenylamine under Ullmann condition was already described, but the product was recovered in low yield.[42] We obtained a similar low yield (ca. 30%) under Hartwig−Buchwald condition, by reacting aniline with 2 equiv of 1-bromo-4-fluorobenzene. When the reaction was carried out with an excess of dihaloarene, however, we found that the secondary amine *N*-(4-fluorophen-1-yl)benzeneamine (**9**) occurred as the main product in very good yield (93%). Subsequently, by reacting **9** with an excess of 1-bromo-4-fluorobenzene under the same condition of cross-coupling reaction, *N*,*N*-bis(4-fluorophen-1-yl)benzeneamine (**10**) could be obtained in very good yield (93%, 86% over 2 steps). The selective bromination with *N*-bromosuccinimide (**11**) followed by reaction with 2-isopropoxy-4,4,5,5-tetramethyl-1,3,2-dioxaborolane gave the boronic ester derivative **12**. The final products **1** and **2** were prepared by Suzuki cross-coupling reaction between **12** and the corresponding fluorene or spirobifluorene core (**7** or **8**, respectively), with 67% and 78% yield, respectively.

2,7-bis(4-(*N*,*N*-bis(4-methylphenyl)amino)phen-1-yl)-9,9-dimethyl-9*H*-fluorene (**3**), 2,7-bis(4-(*N*,*N*-bis(4-methylphenyl)-

DOI: 10.1021/jacs.6b12247
J. Am. Chem. Soc. 2017, 139, 2060−2069

Scheme 2. Synthetic Route for the Synthesis of 3−6

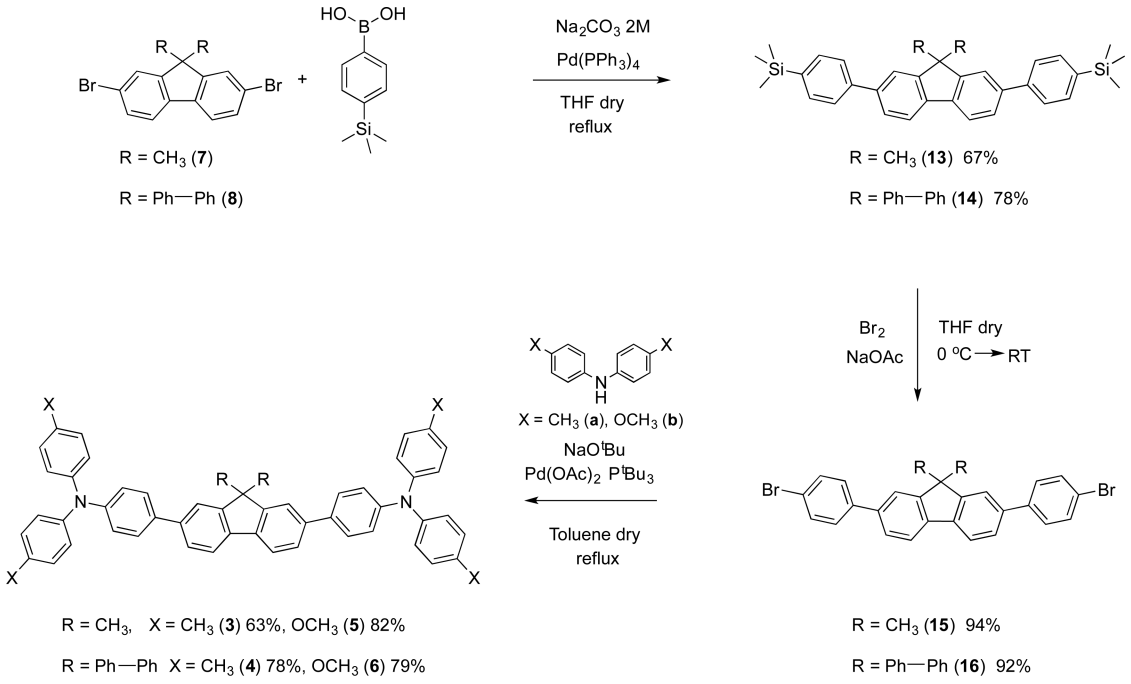

amino)phen-1-yl)-9,9′-spirobifluorene (**4**), 2,7-bis(4-(*N*,*N*-bis-(4-methoxyphenyl)amino)phen-1-yl)-9,9-dimethyl-9*H*-fluorene (**5**) and 2,7-bis(4-(*N*,*N*-bis(4-methoxyphenyl)amino)phen-1-yl)-9,9′-spirobifluorene (**6**) were prepared by starting from the commercially available bis(4-methylphenyl)amine and bis(4-methoxyphenyl)amine (Scheme 2). The first step was a Suzuki reaction between the core and 4-(trimethylsilyl)-phenylboronic acid to give **13** and **14**. The presence of the trimethylsilyl protecting groups allowed introducing the halogen atoms selectively at the *para*-position of the two phenyl rings in two steps with good yield (compounds **15** and **16**), thereby avoiding formation of multibrominate compounds. The sought compounds **3**−**6** were obtained through C−N bond formation between **15** or **16** with the appropriate secondary amine (**a**, (bis(4-methylphenyl)amine; **b**, bis(4-methoxyphenyl)amine) under Hartwig−Buchwald cross-coupling conditions.[43] After column purification, the products were recovered in good yield (**3**, 63%; **4**, 78%; **5**, 82%; **6**, 79%).

Photophysical Characterization. Figure 1a shows the absorption spectra of **1**−**6**. The presence of different *para*-substituents on the triphenylamine groups does not substantially affect the absorption and thus the energetics of the systems. The spectra display a similar pattern characterized by a single absorption band centered in the UVA region (Table 1) and attributed to π-π* transitions of the conjugate system.[33] Compared to the spectra of fluorene **17** and spirobifluorene **18**, in which the triphenylamines are unsubstituted on the external rings,[33] the presence of the electron-withdrawing fluorine in **1** and **2** induces a hypsochromic effect in the absorption band, whereas the presence of electron-donor substituents (Me in **3** and **4**, and OMe in **5** and **6**) induces a bathochromic effect, which is particularly evident for the methoxy group (Table 1). The PL spectra (Figure 1b) display a more pronounced dependence on the triphenylamine *para*-substituents. In the fluorene series, as one goes from **1** to **5** the band maximum shifts from 445 to 500 nm, with a Stokes shift increasing from 77 (**1**) to 118 (**5**) nm. A similar although more pronounced

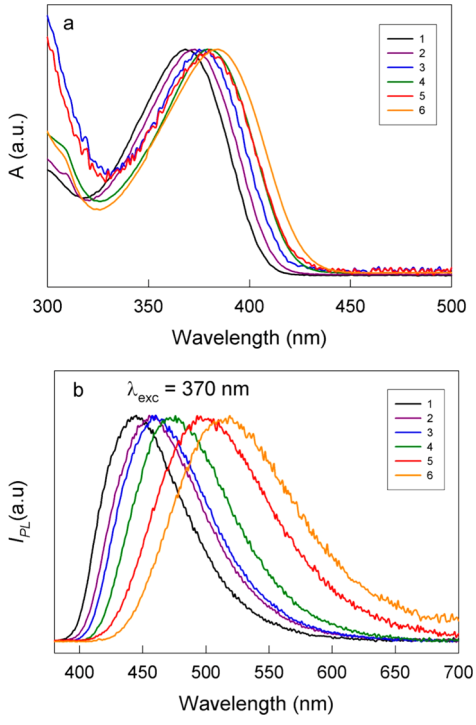

Figure 1. (a) Absorption spectra of 10^{-6} M **1**−**6** in DMF. (b) Emission spectra of 10^{-6} M **1**−**6** in DMF, excited at 370 nm. The peaks were normalized for the peak intensity.

trend is observed for the spirobifluorene series, as the emission maximum shifts from 458 for **2** to 518 nm for **6**, and the corresponding Stokes shift increases from 86 to 134 nm. Noteworthy, both absorption and emission maxima are appreciably red-shifted relative to those of comparable *para*-substitued triphenylamine[32a] and fluorene and spirobifluorene[44−47] derivatives. In **1**−**6**, fine-tuning of the PL emission from blue to green is attributed to the increasing donor

DOI: 10.1021/jacs.6b12247
J. Am. Chem. Soc. 2017, 139, 2060−2069

Table 1. Photophysical Data

comp	Abs λ_{max} (nm)	$\varepsilon \times 10^4$ (M^{-1} cm^{-1})	PL λ_{max} (nm)	absolute QY_{PL} (%)	τ (ns)
1	368	6.611	445	86	1.3
2	372	7.063	458	89	1.6
17[a]	371	6.537	451	81	1.2
18[a]	374	7.302	456	87	1.3
3	378	6.531	458	86	1.7
4	380	7.135	472	87	2.1
5	382	6.108	500	81	3.2
6	384	7.218	518	79	3.2

[a]From ref 33.

strength of the substituents in the *para*-position of the external triphenylamine rings. The observed shifts are also associated with a variation in the polarity of the excited states, as supported by measurements performed in a less polar solvent, such as dichloromethane (see Figure S1 and Table S1 in the Supporting Information).

As one goes from DMF to dichloromethane, the decrease in solvent polarity affects the absorption maximum of the ground state only marginally, with a difference of only 5, 2, and 3 nm for molecules **2**, **4** and **6**, respectively. On the other hand, the PL spectra show a more pronounced bathochromic shift in DMF that increases with the increase in donor strength of the *para*-substituent. The excited state of these molecules has thus a higher charge-separation character than the ground state. In DMF, this stabilization results in a larger red shift in the emission spectra and in a larger Stokes shift compared to a less polar solvent.[48]

Regarding the difference between each pair of the fluorene/spirobifluorene systems, the spirobifluorene compounds are always red-shifted in both absorption and PL emission spectra. This points to the existence of some conjugation between the two fluorenyl moieties, which our results show to be strong enough to cause a decrease of the HOMO−LUMO energy gap. We attribute this interaction to spiroconjugation.[49] It is also worth noting that, independently of the specific substituent and pair system, a very high absolute PL quantum yield (QY_{PL}) was consistently observed (80−90%). Finally, Table 1 shows that all luminescence lifetimes are in the ns range, which points to fluorescence as the emission mechanism.

Electrochemistry. The CV experiments were carried out in DMF/0.1 M TBAP at 25 °C. The formal potential ($E°$) values (or, for evidently multielectron waves, apparent $E°$ values) were obtained as the average between the cathodic and anodic peak potentials. Table 2 shows the results obtained for **1**−**6**; for comparison, the data pertaining to **17** and **18**[33] are also included. The 9,9′-dimethylfluorene and spirobifluorene series display similar electrochemical behaviors, as exemplified in Figure 2 for the spirobifluorene series. Whereas the maximum substituent effect on the reduction peaks is modest (at the most, 0.07 V), it is much more pronounced for the electrooxidation: 0.25 and 0.24 V for the 9,9′-dimethylfluorene and spirobifluorene series, respectively. This is easily understood because oxidation directly involves the triphenylamine moieties, where the substituents are varied, in agreement with the trend expected on the basis of the σ_p-Hammett constant values.[50]

For both series, two CV peaks are detected on the negative-going scan (Figure S2). The first peak (R1) shows a peak-to-peak separation ($\Delta E_{p,R1}$) compatible with the reversible

Table 2. Electrochemical Data in DMF/0.1 M TBAP

	$E°_O$[b] (V)	$\Delta E_{p,O}$ (mV)	$\Delta E°_O$[c] (mV)	$E°_{R1}$ (V)	$\Delta E_{p,R1}$ (mV)	$i_{p,O}/i_{p,R1}$[d]	$E°_{R2}$ (V)
1	0.980	84	52	−2.185	72	1.79	−2.417
2	0.971	76	48	−2.136	63	1.77	−2.386
17[a]	0.954	82	51	−2.221	69	1.76	−2.441
18[a]	0.959	78	49	−2.154	67	1.74	−2.393
3	0.880	75	48	−2.213	65	1.74	−2.452
4	0.892	78	50	−2.133	62	1.82	−2.400
5	0.731	74	46	−2.259	60	1.86	−2.489
6	0.740	77	48	−2.184	66	1.79	−2.434

[a]Compounds **17** and **18** were investigated in DMF containing 0.1 M Bu_4NPF_6.[33] [b]This is an apparent $E°_O$ because the peak is caused by oxidation on both triphenylamine units: see text. [c]Difference between the two triphenylamine $E°_O$ values. [d]Absolute ratio at 0.2 V s^{-1}, where $i_{p,R1}$ corresponds to a one-electron process.

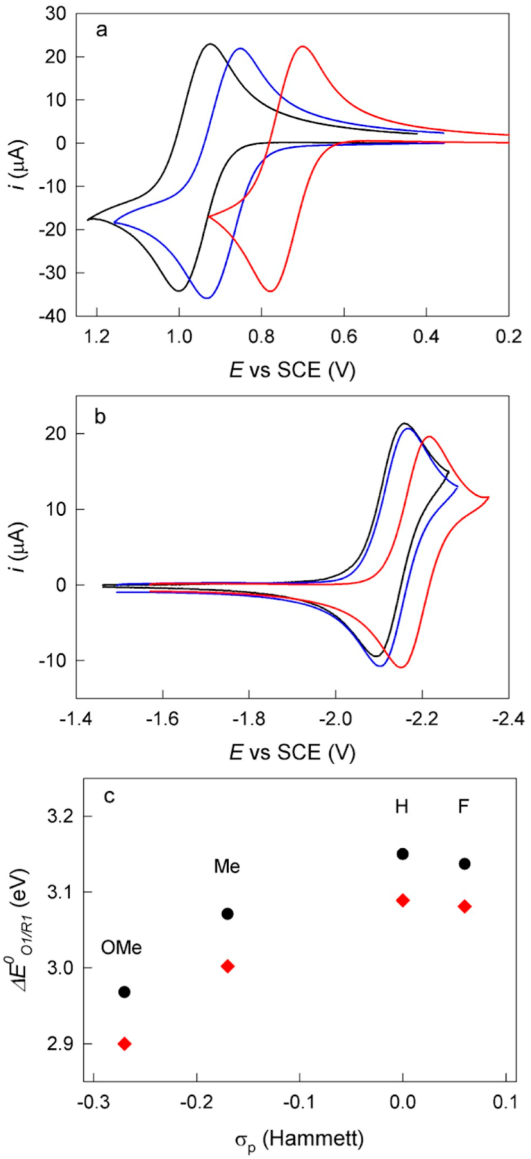

Figure 2. Background-subtracted CVs in DMF/0.1 M TBAP for the oxidation (a) and reduction (b) of 1 mM spirobifluorene derivatives **2** (F, black), **4** (Me, blue), **6** (OMe, red). Scan rate 0.2 V s^{-1}. (c) Correlation between $\Delta E^0_{O1/R1}$ and the Hammett σ_p for fluorene (black dots) and spirobifluorene (red diamonds) series, respectively.

DOI: 10.1021/jacs.6b12247
J. Am. Chem. Soc. 2017, 139, 2060−2069

formation of the fluorene radical anion. The second reduction peak (R2) is partially reversible at low scan rates, and this is attributed to the basicity of the dianion. This peak becomes fully reversible at moderate scan rates, and this allows its E°_{R2} to be determined precisely.

The oxidation peak (O) is fully reversible. For all compounds, however, $\Delta E_{p,O}$ is distinctly larger (Table 2) than the typical one-electron value of 59 mV at 25 °C.[51] It is also significantly larger than the ca. 29 mV separation expected for a fully developed two-electron process, i.e., when the second heterogeneous ET is thermodynamically easier than the first one by at least 0.1 V,[52] an eventuality made possible when the second ET process entails significant conformational changes and specific ion-pair interactions.[53]

The observed $\Delta E_{p,O}$ values are constant in a relatively large scan-rate range and this implies that they truly reflect a thermodynamic effect rather than intrinsically slow heterogeneous ETs or ohmic-drop effects. Finally, for all compounds the ratio between the peak currents of the oxidation and first reduction peaks, $i_{p,O}/i_{p,R1}$, is significantly larger than one. As both reduction processes are clearly one-electron process, $i_{p,O}/i_{p,R1}$ shows that the oxidation peak is the result of a simultaneous oxidation of two amine units.

The occurrence of a two-electron process can be explained by considering that in these type of compounds the two external phenyl moieties are not significantly conjugated to the fluorene core. Generally speaking, when an electron is removed from (or added to) the first of two identical groups on the same molecule, the free energy for the second ET step is function of the extent by which such two moieties interact. If the two relevant orbitals (in the present case, the otherwise degenerate HOMOs) interact through bonds via the bridging group, an energy gap between such orbitals is established. The larger the gap, the larger the through-bond contribution to the overlap between the two frontier orbitals. If there is no interaction, entropic reasons make the second process less favored by a factor $(2RT/F)$ ln 2 = 35.6 mV (at 25 °C).[54] Digital simulation of the experimental CVs provided the ΔE°_{O} values gathered in Table 2 and could also reproduce the experimental $i_{p,O}/i_{p,R1}$ ratios (for example, see Figure S3 for **6**). The values are indeed only slightly larger than 35.6 mV and this indicates that the two triphenylamine moieties are largely electronically independent. Figure 2c shows that the potential difference between the first oxidation and first reduction steps changes with the Hammett σ_p corresponding to the triphenylamine substituents. The difference between the corresponding $\Delta E^{0}_{O1/R1}$ values for the fluorene and the spirobifluorene series is approximately constant, 64 ± 7 mV. The main conclusion of this part of the electrochemical analysis is thus that the two triphenylamine moieties are oxidized at very similar potentials, and the minor interaction between the two redox centers point to two poorly interacting HOMOs.

Comparison (Figure 3) of the CV of **4** with the CVs of spirobifluorene and tris(4-methylphenyl)amine, which provide models for the two electroactive moieties, shows that in **4** the spirobifluorene group is more easily reduced, whereas amine oxidation becomes slightly more difficult. It is also worth noting that the peak currents are substantially different, despite the electrode used and the concentrations were kept constant. Because the diffusion coefficients (D) of **4**, spirobifluorene, and tris(4-methylphenyl)amine are 5.68 × 10^{-6}, 7.28 × 10^{-6}, and 1.46 × 10^{-5} cm^2 s^{-1}, respectively, the oxidation peaks confirm that **4** undergoes a two-electron process. Moreover, the ratio of

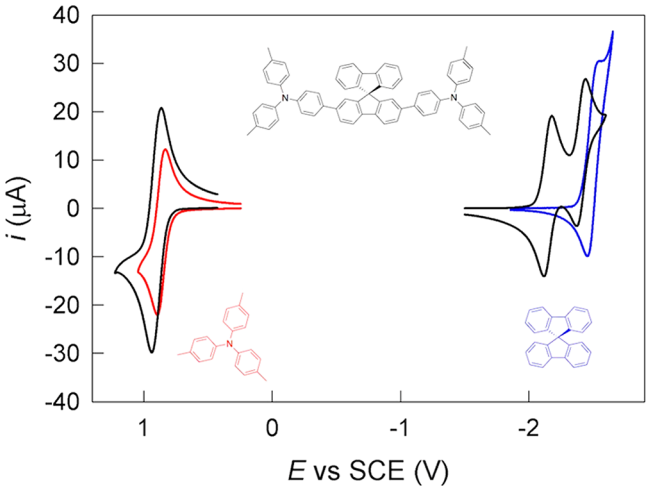

Figure 3. CVs of 1 mM **4** (black), spirobifluorene core (blue), and tris(4-methylphenyl)amine (red) in DMF/0.1 TBAP. Scan rate 0.2 V s^{-1}.

the reduction peak currents of **4** and spirobifluorene, 0.62, is in full agreement with the value calculated for the ratio between the square root of the two diffusion coefficients (i_p is proportional to $D^{1/2}$).[51]

Finally, whereas the difference between the two oxidation potentials is limited, that between the reduction peaks is substantial. Spirobifluorene undergoes reversible reduction at −2.51 V and irreversible reduction (not shown) at −2.77 V, whereas in **4** the first and second reduction steps are easier by 340 and 320 mV, respectively; for reference, the reduction of the simple fluorene systems occurs at −2.69 V. This simple comparison shows that addition of triphenylamines to one of the two fluorene moieties makes reduction of the molecule significantly easier. It also indicates that the LUMO of compounds such as **4** is largely localized onto this specific fluorenyl unit of the spirobifluorene system, rather than on both fluorenyl units; on the contrary, the first two LUMOs of unsubstituted spirobifluorene are degenerate and localized onto either fluorenyl unit.[55] Finally, the modest substituent effect exerted by the specific substitution pattern on the outer triphenylamine rings (Table 2) suggests that the LUMO spreads mostly only on the adjacent phenyl groups of the two triphenylamine moieties.

Theoretical Calculations. We studied the geometrical, electronic, and optical properties of species **2**, **4**, **6**, and **18** by using DFT and TDDFT based methods. Computational modeling provides quantitative information on the molecular structures of the investigated species at the S_0 and S_1 states, the energy and electronic charge distribution of the frontier molecular orbitals, and the UV−vis absorption spectra. This allows assessing the charge flow associated with the S_0−S_1 electronic transition responsible for the lowest energy absorption band.

The ground-state geometries of the investigated spirobifluorene compounds in vacuo and in DMF are very similar. The optimized geometries show mainly a variation in the planarity of the triphenylamine moiety with respect to the fluorene plane, as measured by the dihedral angle α between the latter and the fluorene-linked phenyl of the triphenylamine (Figure S4 and Table S2 in Supporting Information). In the ground state and for all compounds, the average α is 146°−147°, whereas for the S_1 state α markedly increases to 165° (**18**), 166° (**2**), 162° (**4**)

DOI: 10.1021/jacs.6b12247
J. Am. Chem. Soc. 2017, 139, 2060−2069

and 161° (**6**). This shows that more planar systems are attained upon S_0–S_1 excitation; this effect is less pronounced for the compounds carrying electron-donating substituents.

The energy and electronic distribution of the frontier orbitals are quite similar, with slight differences in the occupied orbitals (Figure 4 and Figure S5). For all compounds, the HOMO is delocalized on the triphenylamines and the fluorene unit connecting them (but not on the second spirobifluorene half), showing in **2** and **6** contributions due to the *p* orbitals of F and O atoms, respectively. The tilting of the triphenylamines with respect to the fluorene core lowers the electronic communication between these groups.

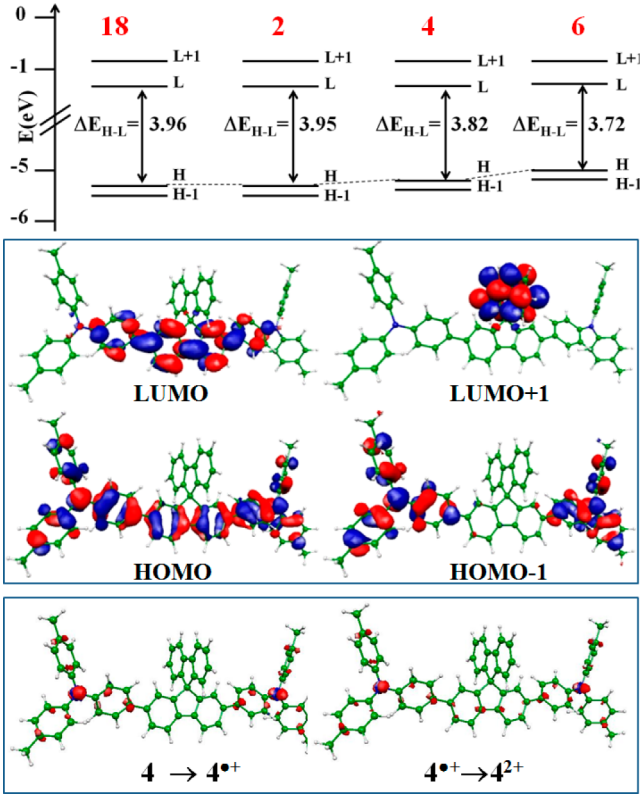

Figure 4. (Top) Frontier orbitals energies (eV) of spirobifluorenes **18**, **2**, **4** and **6** in DMF. (Middle) Electronic isodensity plots (contour value = 0.25) of HOMO/HOMO−1 and LUMO/LUMO+1 of spirobifluorene **4**. (Bottom) Density difference upon the first and second oxidation of **4**; a red (blue) color indicates a decrease (increase) of the electron density upon oxidation.

The LUMO shows bonding character between the fluorene core and the phenyl ring connecting the triphenylamines (Figure 4), in line with the molecules planarization calculated in the excited states. Substitution of hydrogen by fluorine (**18** to **2**) only marginally affects the energy of the frontier molecular orbitals, whereas substitution with the electron-donating Me and OMe (**4** and **6**, respectively) causes a progressive destabilization of the HOMO (and HOMO−1) by ca. 0.25 eV compared to **18**. Instead, the energy of both LUMO and LUMO+1 are virtually unaffected. The HOMO destabilization leads to a slight decrease of the HOMO–LUMO gap (see Figure 4), which ultimately determines the tuning of the optical properties. The simulated absorption spectra in DMF thus evidence a red-shift when moving from H to OMe (Figure S6) in agreement with the experimental observation. This bathochromic shift is related to a larger increase of the dipole moment on going from the ground state to the excited state (Table S3). The computed S_1 excited state is indeed more polar than the ground state, with an increase in polarity difference that follows the order **2** < **18** < **4** < **6**. The main absorption band is originated by a single excitation $S_0 \rightarrow S_1$, which is essentially a HOMO → LUMO transition (ca. 90%). To visualize the $S_0 \rightarrow S_1$ excitation we computed the isodensity plots of the electron density difference between S_1 excited state and the ground state for all the investigated compounds (Figure S6). A charge transfer from the peripheral triphenylamines to the inner fluorene core moiety is observed, suggesting a similar localization of holes/electrons upon oxidation/reduction.

To evaluate electronic charge rearrangement occurring upon oxidation beyond a simple orbital picture, we explicitly calculated the radical cation considered in the electrochemical analysis, $\mathbf{4}^{\bullet+}$ and the doubly oxidized species $\mathbf{4}^{2+}$; similar conclusions hold for all the investigated compounds. These calculations effectively account for the electronic relaxation effects due to oxidation in a more rigorous way than the single orbitals. Notably, for both the first and second oxidation the larger electron-density difference (Figure 4 Bottom) is observed mainly on the nitrogen atoms, and no communication with the rest of the system is evident. These results are, therefore, fully consistent with the outcome of the electrochemical analysis that evidenced the almost independent electrooxidation behavior of the two triphenylamine moieties.

ECL. Figure 5 compares the ECL spectra for **1**–**6**. The ECL spectra were obtained by pulsing the electrode potential between 100 mV past the oxidation peak and 100 mV past the second reduction peak, each step consisting of 25 ms. Radical cations and radical anions annihilated to form an excited state whose subsequent emission signal was integrated for 1 s using a 1 nm slit width. The short exposition time employed to collect the ECL emission spectra indicates that the annihilation process in these molecules is highly efficient. Figure 5 shows

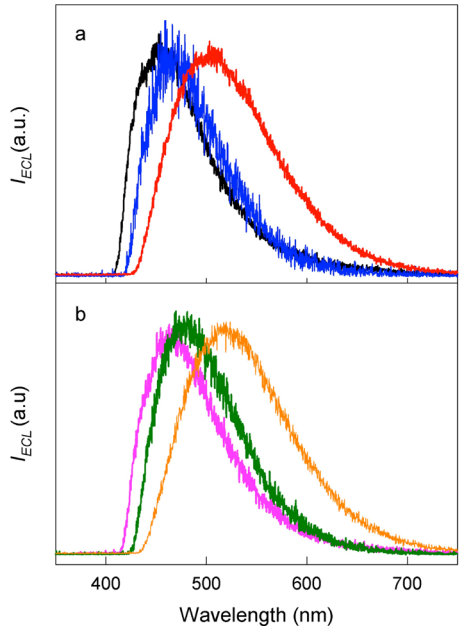

Figure 5. ECL spectra of 1 mM solutions (DMF/0.1 M TBAP) of (graph a) **1** (black), **3** (blue), and **5** (red), or (graph b) **2** (purple), **4** (green), and **6** (orange).

DOI: 10.1021/jacs.6b12247
J. Am. Chem. Soc. 2017, 139, 2060–2069

that for both series of compounds the ECL spectra display one maximum that nearly matches that of the PL pattern (Figure 1b). Similarly to the PL data, the effect of the *para* substituents on the triphenylamine rings is particularly significant, as both types of spectra undergo a red shift when one goes from fluorine to methoxy with a remarkable $\Delta\lambda$ of 67 (ECL) and 73 (PL) nm, respectively. The effect exerted by the substituents is summarized in Figure 6 where the emission wavelength maxima

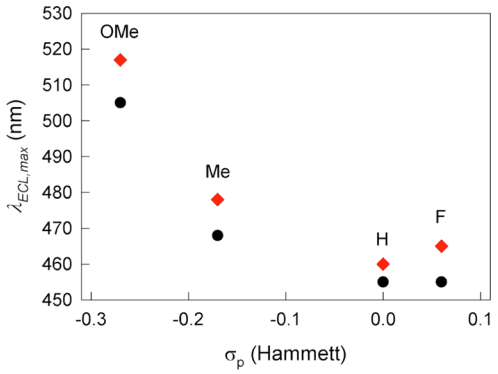

Figure 6. ECL emission wavelength maxima (nm) of fluorene (black dots) and spirobifluorene (red diamonds) derivatives versus σ_p-Hammett.

are plotted against the σ_p-Hammett. For comparison, the data for **17** and **18** are also shown. The emission wavelength maxima are collected in Table 3.

Table 3. ECL Data in DMF/0.1 M TBAP

	ECL λ_{max}	E_s (eV)[a]	$-\Delta H_{ann}$ (eV)[b]	QY_{ECL}[c]
1	455	2.79	3.04 (3.32)	3.5
2	465	2.71	2.98 (3.28)	3.7
17[d]	453, 484	2.75	3.05 (3.32)	3.0
18[d]	450, 493	2.72	2.99 (3.28)	1.7
3	468	2.71	2.97 (3.26)	3.0
4	478	2.63	2.90 (3.22)	2.7
5	505	2.48	2.87 (3.14)	4.2
6	517	2.39	2.80 (3.10)	3.2

[a] E_s estimated from fluorescence emission maximum. [b] $-\Delta H_{ann} = E^0_{O1} - E^0_{R1} - 0.1$; the corresponding values for E^0_{O1}/E^0_{R2} are in parentheses. [c] Relative to DPA, taking QY_{ECL} of DPA = 1. [d] From ref 33.

The ECL quantum yields (QY_{ECL}) were calculated, via a comparative method, as the photons emitted per redox event relative to 9,10-diphenylanthracene (DPA) under the same experimental conditions: for DPA in DMF, QY_{ECL} was determined to be 0.0025.[56] For all compounds we found values higher than DPA (Table 3). To the best of our knowledge, these are among the highest values so far achieved with polyaromatic hydrocarbon compounds emitting in the blue-green region. In terms of QY_{ECL}, no evident effect is brought about by the substituents on the external rings or the passage from the fluorene to the spirobifluorene systems. The emission intensity tends to decrease as the number of pulses increases (Figure S7). However, even after several pulses the light emitted was still so intense to be seen by naked eye and recorded with a smartphone camera (Figure S8 and Video S1 in Supporting Information).

To check the importance of having both the triphenylamines and the fluorene/spirobifluorene centers in the same molecule, we carried out also experiments using spirobifluorene (1 mM) and tris(4-methylphenyl)amine (2 mM), under the same experimental conditions used for 1 mM **4**. We found that when a 25 ms pulse is employed, ECL emission occurs, but the intensity of the light emitted is ~300 times lower than that obtained with **4** (Figure S9). Furthermore, when the pulse time is made slightly longer than 25 ms no ECL occurs for the bimolecular system, whereas compounds **1**–**6** display light emission even for longer pulse times (>200 ms). For simplicity, we now denote triphenylamine (as a single molecule or as triphenylamine units) and spirobifluorene (again, as a single molecule or as a bridge) as TPA and SBF, respectively. During the negative step, just before the potential is stepped positively, the surface concentration of $SBF^{\bullet-}$ is at its maximum value. Upon positive electrode polarization, $TPA^{\bullet+}$ is generated and, concomitantly, the surface concentration of $SBF^{\bullet-}$ drops to zero because of its concurrent quantitative reoxidation to SBF.

At this stage, the difference between the two separate species and **4** is that in the latter two $TPA^{\bullet+}$ radical cations form simultaneously: due to the slightly favored comproportionation reaction (for **4**, the comproportionation equilibrium constant is K_c = 7.0; for the whole series, K_c is in the range from 6.5 to 7.6), some dication reacts with a neutral molecule to form two separate radical cations. For both molecular systems, the diffusion layer is still rich of $SBF^{\bullet-}$ that can exchange one electron with the $TPA^{\bullet+}$ (or with one of the $TPA^{\bullet+}$ moieties in **4**) diffusing toward the bulk. For the two separated ions, annihilation generates the excited state TPA*. For the complex systems, on the other hand, the HOMO and the LUMO are located in substantially different parts of the molecule and, therefore, annihilation can be seen as generating a radical-ion pair consisting of a TPA oxidized moiety and a SBF (or fluorene) reduced moiety. Consequently, the same excited-state species obtained upon direct light absorption in the PL experiments forms.

The process can be described as an intramolecular charge-transfer emission. The different ECL efficiency in the two types of system is thus related to the presence of the fluorene-type bridge, two triphenylamine units in the same molecule, and sufficiently separated relevant orbitals.

To understand which pathway is followed by ECL in the fluorene and spirobifluorene systems, we calculated the energy of the excited state from the fluorescence spectrum using equation E_s (eV) = 1239.81/λ, where λ (in nm) is the wavelength at the maximum emission peak.[1] Table 3 shows the estimated values for the energy of the first singlet excited state. The annihilation enthalpy ΔH_{ann} (in eV) can be calculated as $\Delta H_{ann} = -(E^0_{O1} - E^0_{R1} - 0.1)$, where the −0.1 eV term is a commonly adopted entropy correction.[1] Table 3 shows that for all compounds the energy associated with $-\Delta H_{ann}$ is larger than E_s and, therefore, all these systems are energy sufficient. This points to luminescence as arising from a species in a singlet excited state, and thus that the process follows the S-route.[1] This is in keeping with the similarity between the ECL and PL results and the PL luminescence lifetimes.

It is finally worth noting that for all compounds the ECL intensity decreases by pulsing to potentials of the first reduction peak (Figure 7). This behavior appears to be associated with the stoichiometry of the radical ions present in solution.[57,58] Whereas at the potentials of the positive step a dication forms (each amine moiety undergoes a nearly independent one-

DOI: 10.1021/jacs.6b12247
J. Am. Chem. Soc. 2017, 139, 2060–2069

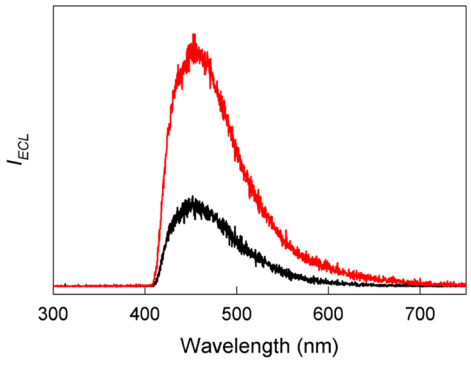

Figure 7. ECL spectra of **1** collected by pulsing between the oxidation and the first (black) or second (red) reduction peak.

electron oxidation), in the negative step the radical anion or the dianion is produced selectively; the latter undergoes a favored ET with a neutral molecule (for the whole series, K_c is between 5.2×10^3 and 3.3×10^4) to form two radical anions. By pulsing between the oxidation and the first reduction peaks, excess diradical dications and radical cations (because of the comproportionation reaction) form in the reaction layer. When the spectrum is recorded by including the second reduction peak, the stoichiometry of radical ions is balanced and the annihilation reaction of the dication-dianion pair produces a higher intensity ECL emission.

CONCLUSIONS

We have described the synthesis, photophysics, computational analysis, and electrochemical behavior of efficient ECL emitting bifunctional dyes consisting of a fluorene or spirobifluorene core linked to *para*-substituted triphenylamines. The compounds were prepared in good yield, through two different approaches, by using Suzuki or Hartwig–Buchwald cross-coupling reaction. All compounds show blue-green emission, with high quantum yields. ECL spectra almost match those obtained by photoluminescence, and ECL efficiency is higher than for the standard ECL emitter 9,10-diphenylanthracene. The effect of the substituent groups on the amine moieties allows fine-tuning of the emission properties with a remarkable $\Delta\lambda$ of 73 (PL) and 67 (ECL) nm, respectively. Analysis of the results indicates that all systems are energy-sufficient and ECL emission is caused by the singlet-excited state obtained by the S-route. This class of ECL systems have the merits of showing (i) reversible and stable electrochemical behavior, (ii) very high PL quantum yields, and (iii) high ECL efficiency without formation of excimers. The investigated molecules demonstrate the effective possibility to design highly emitting systems for ECL applications with tunable emission wavelength. Concerning possible developments, we note that although both the fluorene and the spirobifluorene systems show very nice PL and ECL behaviors, the spirobifluorene system offers the chance of introducing suitable electron-withdrawing substituents in second fluorene moiety. By this strategy, an even more effective separation of HOMO and LUMO should be attained, resulting in a further fine-tuned red shift.

ASSOCIATED CONTENT

Supporting Information

The Supporting Information is available free of charge on the ACS Publications website at DOI: 10.1021/jacs.6b12247.

Full experimental details on methods and syntheses, and further photophysical and electrochemical characterization results (PDF)

Video S1 (AVI)

AUTHOR INFORMATION

Corresponding Authors

*fabio.rizzo@istm.cnr.it

*federico.polo@cro.it

*flavio.maran@unipd.it

ORCID

Fabio Rizzo: 0000-0003-4045-2653

Federico Polo: 0000-0003-4638-396X

Present Address

#National Cancer Institute–Centro di Riferimento Oncologico, via Franco Gallini 2, 33081 Aviano, Italy.

Notes

The authors declare no competing financial interest.

ACKNOWLEDGMENTS

This work was financially supported by AIRC (FM, Project 12214: Innovative Tools for cancer risk assessment and early diagnosis −5 per mille) and FIRB-MIUR (Project RBAP114AMK: RINAME—Integrated Network for Nano-Medicine).

REFERENCES

(1) *Electrogenerated Chemiluminescence*; Bard, A. J., Ed.; Marcel Dekker: New York, 2004.

(2) Marcus, R. A.; Sutin, N. *Biochim. Biophys. Acta, Rev. Bioenerg.* **1985**, *811*, 265–322.

(3) Ludvík, J. *J. Solid State Electrochem.* **2011**, *15*, 2065–2081.

(4) Antonello, S.; Maran, F. *J. Am. Chem. Soc.* **1999**, *121*, 9668–9676.

(5) Antonello, S.; Hesari, M.; Polo, F.; Maran, F. *Nanoscale* **2012**, *4*, 5333–5342.

(6) Richter, M. M. *Chem. Rev.* **2004**, *104*, 3003–3036 and references therein.

(7) Miao, W. *Chem. Rev.* **2008**, *108*, 2506–2538 and references therein.

(8) Sardesai, N. P.; Barron, J. C.; Rusling, J. F. *Anal. Chem.* **2011**, *83*, 6698–6703.

(9) Xu, D.; Adac hi, C. *Appl. Phys. Lett.* **2009**, *95*, 053304.

(10) Hirata, S.; Kubota, K.; Jung, H. H.; Hirata, O.; Goushi, K.; Yahiro, M.; Adachi, C. *Adv. Mater.* **2011**, *23*, 889–893.

(11) Kasahara, T.; Matsunami, S.; Edura, T.; Ishimatsu, R.; Oshima, J.; Tsuwaki, M.; Imato, T.; Shoji, S.; Adachi, C.; Mizuno, J. *Sens. Actuators, A* **2014**, *214*, 225–229.

(12) (a) Barbante, G. J.; Hogan, C. F.; Mechler, A.; Hughes, A. B. *J. Mater. Chem.* **2010**, *20*, 891–899. (b) Filiatrault, H. L.; Porteous, G. C.; Carmichael, R. S.; Davidson, G J. E.; Carmichael, T. B. *Adv. Mater.* **2012**, *24*, 2673–2678.

(13) Nepomnyashchii, A. B.; Bard, A. J. *Acc. Chem. Res.* **2012**, *45*, 1844–1853.

(14) Qi, H.; Teesdale, J. J.; Pupillo, R. C.; Rosenthal, J.; Bard, A. J. *J. Am. Chem. Soc.* **2013**, *135*, 13558–13566.

(15) Ishimatsu, R.; Matsunami, S.; Kasahara, T.; Mizuno, J.; Edura, T.; Adachi, C.; Nakano, K.; Imato, T. *Angew. Chem., Int. Ed.* **2014**, *53*, 6993–6996.

(16) Fernández-Hernández, J.; Longhi, E.; Cysewski, R.; Polo, F.; Josel, H.-P.; De Cola, L. *Anal. Chem.* **2016**, *88*, 4174–4178.

(17) Zanarini, S.; Felici, M.; Valenti, G.; Marcaccio, M.; Prodi, L.; Bonacchi, S.; Contreras-Carballada, P.; Williams, R. M.; Feiters, M. C.; Nolte, R. J. M.; De Cola, L.; Paolucci, F. *Chem. - Eur. J.* **2011**, *17*, 4640–4647.

DOI: 10.1021/jacs.6b12247
J. Am. Chem. Soc. 2017, 139, 2060–2069

(18) Schmittel, M.; Shu, Q.; Cinar, M. E. *Dalton Trans.* **2012**, *41*, 6064−6068.
(19) Reid, E. F.; Cook, V. C.; Wilson, D. J. D.; Hogan, C. F. *Chem. - Eur. J.* **2013**, *19*, 15907−15917.
(20) Valenti, G.; Rampazzo, E.; Bonacchi, S.; Khajvand, T.; Juris, R.; Montalti, M.; Marcaccio, M.; Paolucci, F.; Prodi, L. *Chem. Commun.* **2012**, *48*, 4187−4189.
(21) Lingling, L.; Hongying, L.; Yuanyuan, S.; Jianrong, Z.; Jun-Jie, Z. *Anal. Chem.* **2011**, *83*, 661−665.
(22) Li, H.; Daniel, J.; Verlhac, J.-B.; Blanchard-Desce, M.; Sojic, N. *Chem. - Eur. J.* **2016**, *22*, 12702−12714.
(23) Valenti, G.; Bruno, C.; Rapino, S.; Fiorani, A.; Jackson, E. A.; Scott, L. T.; Paolucci, F.; Marcaccio, M. *J. Phys. Chem. C* **2010**, *114*, 19467−19472.
(24) Kerr, E.; Doeven, E. H.; Barbante, G. J.; Hogan, C. F.; Bower, D. J.; Donnelly, P. S.; Connell, T. U.; Francis, P. S. *Chem. Sci.* **2015**, *6*, 472−479.
(25) (a) Omer, K. M.; Ku, S.-Y.; Wong, K.-T.; Bard, A. J. *J. Am. Chem. Soc.* **2009**, *131*, 10733−10741. (b) Omer, K. M.; Ku, S.-Y.; Wong, K.-T.; Bard, A. J. *Angew. Chem., Int. Ed.* **2009**, *48*, 9300−9303. (c) Omer, K. M.; Ku, S.-Y.; Cheng, J.-Z.; Chou, S.-H.; Wong, K.-T.; Bard, A. J. *J. Am. Chem. Soc.* **2011**, *133*, 5492−5499.
(26) Swanick, K. N.; Price, J. T.; Jones, N. D.; Ding, Z. *J. Org. Chem.* **2012**, *77*, 5646−5655.
(27) Natarajan, P.; Schmittel, M. *J. Org. Chem.* **2013**, *78*, 10383−10394.
(28) Adam, C.; Wallabregue, A.; Li, H.; Gouin, J.; Vanel, R.; Grass, S.; Bosson, J.; Bouffier, L.; Lacour, J.; Sojic, N. *Chem. - Eur. J.* **2015**, *21*, 19243−19249.
(29) Ketter, J. B.; Wightman, R. M. *J. Am. Chem. Soc.* **2004**, *126*, 10183−10189.
(30) (a) Fungo, F.; Wong, K.-T.; Ku, S.-Y.; Hung, Y.-Y.; Bard, A. J. *J. Phys. Chem. B* **2005**, *109*, 3984−3989. (b) Qi, H.; Chen, Y.-H.; Cheng, C.-H.; Bard, A. J. *J. Am. Chem. Soc.* **2013**, *135*, 9041−9049.
(31) (a) Elangovan, A.; Yang, S.-W.; Lin, J.-H.; Kao, K.-M.; Ho, T.-I. *Org. Biomol. Chem.* **2004**, *2*, 1597−1602. (b) Elangovan, A.; Lin, J.-H.; Yang, S.-W.; Hsu, H.-Y.; Ho, T.-I. *J. Org. Chem.* **2004**, *69*, 8086−8092. (c) Ho, T.-I.; Elangovan, A.; Hsu, H.-Y.; Yang, S.-W. *J. Phys. Chem. B* **2005**, *109*, 8626−8633.
(32) (a) Quinton, C.; Alain-Rizzo, V.; Dumas-Verdes, C.; Miomandre, F.; Clavier, G.; Audebert, P. *RSC Adv.* **2014**, *4*, 34332−34342. (b) Quinton, C.; Alain-Rizzo, V.; Dumas-Verdes, C.; Miomandre, F.; Clavier, G.; Audebert, P. *Chem. - Eur. J.* **2015**, *21*, 2230−2240.
(33) Polo, F.; Rizzo, F.; Veiga-Gutierrez, M.; De Cola, L.; Quici, S. *J. Am. Chem. Soc.* **2012**, *134*, 15402−15409.
(34) Antonello, S.; Musumeci, M.; Wayner, D. D. M.; Maran, F. *J. Am. Chem. Soc.* **1997**, *119*, 9541−9549.
(35) Meneses, A. B.; Antonello, S.; Arévalo, M.-C; Maran, F. *Electroanalysis* **2006**, *18*, 363−370.
(36) Frisch, M. J.; Trucks, G. W.; Schlegel, H. B.; Scuseria, G. E.; Robb, M. A.; Cheeseman, J. R.; Scalmani, G.; Barone, V.; Mennucci, B.; Petersson, G. A.; Nakatsuji, H.; Caricato, M.; Li, X.; Hratchian, H. P.; Izmaylov, A. F.; Bloino, J.; Zheng, G.; Sonnenberg, J. L.; Hada, M.; Ehara, M.; Toyota, K.; Fukuda, R.; Hasegawa, J.; Ishida, M.; Nakajima, T.; Honda, Y.; Kitao, O.; Nakai, H.; Vreven, T.; Montgomery, J. A., Jr.; Peralta, J. E.; Ogliaro, F.; Bearpark, M.; Heyd, J. J.; Brothers, E.; Kudin, K. N.; Staroverov, V. N.; Kobayashi, R.; Normand, J.; Raghavachari, K.; Rendell, A.; Burant, J. C.; Iyengar, S. S.; Tomasi, J.; Cossi, M.; Rega, N.; Millam, J. M.; Klene, M.; Knox, J. E.; Cross, J. B.; Bakken, V.; Adamo, C.; Jaramillo, J.; Gomperts, R.; Stratmann, R. E.; Yazyev, O.; Austin, A. J.; Cammi, R.; Pomelli, C.; Ochterski, J. W.; Martin, R. L.; Morokuma, K.; Zakrzewski, V. G.; Voth, G. A.; Salvador, P.; Dannenberg, J. J.; Dapprich, S.; Daniels, A. D.; Farkas, Ö.; Foresman, J. B.; Ortiz, J. V.; Cioslowski, J.; Fox, D. J. *Gaussian 09*, Revision E.01; Gaussian, Inc.: Wallingford, CT, 2009.
(37) Zhao, Y.; Truhlar, D. G. *Theor. Chem. Acc.* **2008**, *120*, 215−41.
(38) Petersson, G. A.; Bennett, A.; Tensfeldt, T. G.; Al-Laham, M. A.; Shirley, W. A.; Mantzaris, J. *J. Chem. Phys.* **1988**, *89*, 2193−218.
(39) (a) Miertus, S.; Scrocco, E.; Tomasi, J. *Chem. Phys.* **1981**, *55*, 117−129. (b) Cossi, M.; Barone, V.; Cammi, R.; Tomasi, J. *Chem. Phys. Lett.* **1996**, *255*, 327−335.
(40) Saroja, G.; Pingzhu, Z.; Ernsting, N. P.; Liebscher, J. *J. Org. Chem.* **2004**, *69*, 987−990.
(41) Yu, W.-L.; Pei, J.; Huang, W.; Heeger, A. J. *Adv. Mater.* **2000**, *12*, 828−831.
(42) He, Z.; Wong, W.-Y.; Yu, X.; Kwok, H.-S.; Lin, Z. *Inorg. Chem.* **2006**, *45*, 10922−10937.
(43) Hartwig, J. F.; Kawatsura, M.; Haula, S. I.; Shaughnessey, K. H.; Alcazar-Roman, L. M. *J. Org. Chem.* **1999**, *64*, 5575−5580.
(44) Wong, K.-T.; Chien, Y.-Y.; Chen, R.-T.; Wang, C.-F.; Lin, Y.-T.; Chiang, H.-H.; Hsieh, P.-Y.; Wu, C.-C.; Chou, C. H.; Su, Y. O.; Lee, G.-H.; Peng, S.-M. *J. Am. Chem. Soc.* **2002**, *124*, 11576−11577.
(45) Kotaka, H.; Konishi, G.-i; Mizuno, K. *Tetrahedron Lett.* **2010**, *51*, 181−184.
(46) Yi, C.; Sun, Y.; Song, B.; Tian, W.; Qi, Q.; Zheng, Y.; Dai, Y.; Jiang, W. *Nanotechnology* **2013**, *24*, 435704.
(47) Tao, S.; Peng, Z.; Zhang, Z.; Wang, P.; Lee, C.-S.; Lee, S.-T. *Adv. Funct. Mater.* **2005**, *15*, 1716−1721.
(48) *Principles of Fluorescence Spectroscopy*, 3rd ed.; Lakowicz, J. R., Ed.; Springer-Verlag, 2006.
(49) Boo, B. H.; Choi, Y. S.; Kim, T.-S.; Kang, S. K.; Kang, Y. H.; Lee, S. Y. *J. Mol. Struct.: THEOCHEM* **1996**, *377*, 129−136.
(50) Hansch, C.; Leo, A.; Taft, R. W. *Chem. Rev.* **1991**, *91*, 165−195.
(51) Nicholson, R. S.; Shain, I. *Anal. Chem.* **1964**, *36*, 706−723.
(52) Polcyn, D. S.; Shain, I. *Anal. Chem.* **1966**, *38*, 370−375.
(53) Evans, D. H. *Chem. Rev.* **2008**, *108*, 2113−2144.
(54) Ammar, F.; Saveant, J.-M. *J. Electroanal. Chem. Interfacial Electrochem.* **1973**, *47*, 215−221.
(55) Thiery, S.; Tondelier, D.; Declairieux, C.; Seo, G.; Geffroy, B.; Jeannin, O.; Rault-Berthelot, J.; Métivier, R.; Poriel, C. *J. Mater. Chem. C* **2014**, *2*, 4156−4166.
(56) Bezman, R.; Faulkner, L. R. *J. Am. Chem. Soc.* **1972**, *94*, 6317−6323.
(57) Shen, M.; Rodríguez-López, J.; Huang, J.; Liu, Q.; Zhu, X.-H.; Bard, A. J. *J. Am. Chem. Soc.* **2010**, *132*, 13453−13461.
(58) Shen, M.; Rodríguez-López, J.; Lee, Y.-T.; Chen, C.-T.; Fan, F.-R. F.; Bard, A. J. *J. Phys. Chem. C* **2010**, *114*, 9772−9780.

DOI: 10.1021/jacs.6b12247
J. Am. Chem. Soc. 2017, 139, 2060−2069